



OPEN

Identification of new pillared-layered carbon nitride materials at high pressure

Ashkan Salamat^{1,2}, Malek Deifallah², Raul Quesada Cabrera², Furio Corà² & Paul F. McMillan²¹Lyman Laboratory of Physics, Harvard University, Cambridge, MA 02138, USA, ²Department of Chemistry, University College London, London WC1H 0AJ, UK.

The compression of the layered carbon nitride $C_6N_9H_3 \cdot HCl$ was studied experimentally and with density functional theory (DFT) methods. This material has a polytriazine imide structure with Cl^- ions contained within $C_{12}N_{12}$ voids in the layers. The data indicate the onset of layer buckling accompanied by movement of the Cl^- ions out of the planes beginning above 10–20 GPa followed by an abrupt change in the diffraction pattern and c axis spacing associated with formation of a new interlayer bonded phase. The transition pressure is calculated to be 47 GPa for the ideal structures. The new material has mixed sp^2 – sp^3 hybridization among the C and N atoms and it provides the first example of a pillared-layered carbon nitride material that combines the functional properties of the graphitic-like form with improved mechanical strength. Similar behavior is predicted to occur for Cl-free structures at lower pressures.

High pressure investigations of carbon nitride materials have been stimulated by theoretical predictions that dense sp^3 -bonded C_3N_4 phases would display low compressibility and high hardness values^{1,2}. Despite many synthesis attempts including use of high pressure the formation of crystalline C_3N_4 polymorphs remains an elusive goal. However an sp^3 -bonded carbon nitride imide C_2N_3H with a defective wurtzite structure has been produced in laser-heated diamond anvil cell (DAC) experiments and this material was recoverable to ambient conditions^{3,4}. Low density sp^2 bonded polymeric or layered graphitic carbon nitride materials (g-CNMs) are also well known⁵ and these have attracted attention as metal-free redox catalysts, photocatalysts and electroceramic materials^{6,7}. They also provide precursors for investigation of pressure-induced transformations into dense sp^3 bonded phases. We investigated the room temperature compression behavior of one such well-characterized g-CNM of composition $C_6N_9H_3 \cdot HCl$ ⁸ to 70 GPa using synchrotron X-ray diffraction experiments in a diamond anvil cell (DAC) combined with density functional theory (DFT) calculations carried out to 100 GPa. The combined experimental and theoretical results indicate the initial onset of layer buckling and movement of the Cl^- ions out of their sites within the planes followed by a phase transformation into a structure containing interlayer C–N bonds between sp^3 hybridized atoms. The new material constitutes a new example of a pillared-layered gCNM with mixed sp^2 – sp^3 bonding. Related bonding changes have been recorded in graphitic C and BN materials at high pressure^{9–14}.

A large class of oligomeric, polymeric and graphitic carbon nitride materials are determined to have structures based on heptazine (tri-*s*-triazine, C_6N_7) rings linked by $-N=$ or $-NH-$ groups¹⁵. A second structural motif based on polymerized triazine (C_3N_3) units is found among graphitic nanocrystalline C_3N_4 prepared by chemical vapor deposition¹⁶. Triazine units are also the building blocks in bulk crystalline compounds synthesized from precursors including melamine ($C_3N_6H_6$) and cyanuric chloride ($C_3N_3Cl_3$) under high-*P,T* conditions (0.5–3 GPa, 300–500 °C). Further studies have obtained crystalline graphitic polytriazine imides (PTI) with related structures by reactions in molten salt mixtures (e.g. KCl–LiCl eutectics)^{5,17}. The *s*-triazine rings linked by bridging $-N=$ or $-NH-$ units lead to large voids within the graphitic layers. In the case of $C_6N_9H_3 \cdot HCl$ studied here the Cl^- ions occupy the centers of the voids at ambient pressure. The layers are stacked to provide an alternating pattern of triazine and $C_{12}N_{12}$ rings along the c axis (Fig. 1).

Results

Experimental findings. The starting compound g- $C_6N_9H_3 \cdot HCl$ is described by a hexagonal unit cell with $P6_3/m$ symmetry (Fig. 1)^{8,18}. The X-ray patterns at low pressure (Fig. 2) are dominated by the (002) interlayer reflection at $2\theta \sim 8^\circ$ that is indicative of a layered graphite-like structure with an ABAB stacking along the c axis. The polytriazine imide layers contain $C_{12}N_{12}H_3$ voids hosting Cl^- ions derived from the synthesis reaction between melamine and cyanuric chloride, and additional H^+ ions are bound to the N atoms of the triazine

SUBJECT AREAS:
SOLID-STATE CHEMISTRY
MECHANICAL PROPERTIES
ELECTRONIC MATERIALS
ELECTRONIC PROPERTIES AND MATERIALS

Received
24 May 2013

Accepted
17 June 2013

Published
2 July 2013

Correspondence and requests for materials should be addressed to A.S. (salamat@physics.harvard.edu); F.C. (f.cora@ucl.ac.uk) or P.F.M. (p.f.mcmillan@ucl.ac.uk)

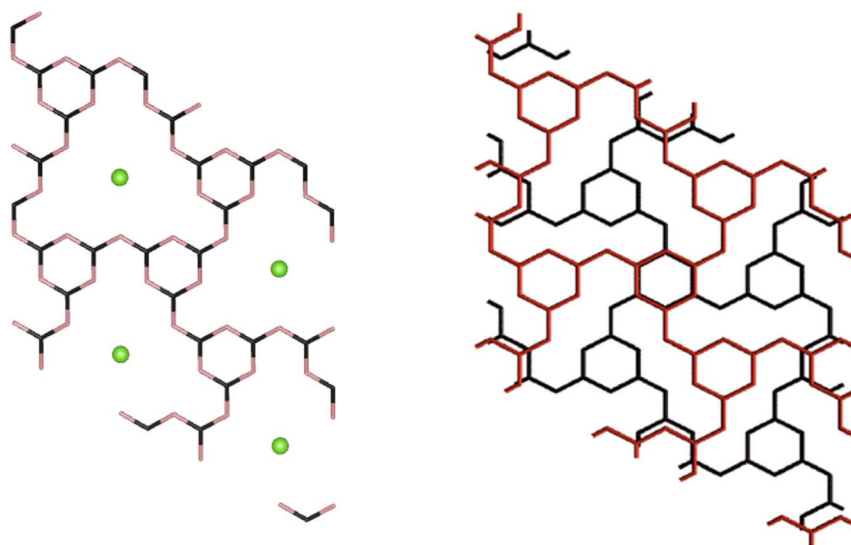


Figure 1 | Structural features of graphitic $C_6N_9H_3 \cdot HCl$ at ambient pressure. (left) Top view of one plane of the structure showing the triazine (C_3N_3) rings connected by $-NH-$ groups to form large $C_{12}N_{12}$ voids that are occupied by Cl^- ions. The accompanying extra H^+ ion is attached to one of six possible N positions from the triazine units surrounding the large ring^{6,16}. The H atoms have been omitted for clarity. (right) View down c of two adjacent layers of the structure showing the ABAB stacking sequence that places one triazine ring above the $C_{12}N_{12}$ void in successive planes. The H and Cl species are not shown for clarity.

rings^{8,18}. Only one of six available N sites is protonated in this way so that the $P6_3/m$ space group used to analyze the data represents a spatially averaged solution. The ABAB stacking of the graphitic layers creates a structure in which one half of the triazine rings within each layer is positioned above or below $C_{12}N_{12}$ voids in adjacent layers, while the others overlap triazine rings in the layers above and below (Fig. 1).

The prominent (002) interlayer reflection shifts rapidly to smaller d spacing ($2\theta \sim 10^\circ$) with increasing pressure (Fig. 2). Above 10 GPa the diffraction peaks become significantly broadened but the general features of the graphitic material are still recognizable up to $P \sim 36$ GPa. However at $P = 40$ GPa the nature of the pattern has changed to become dominated by a main broad asymmetric peak near $13^\circ 2\theta$. This result signals a structural change into a new high-density form (Fig. 2). After the transformation has occurred the peak positions vary little with continued compression up to 70 GPa indicating that the high pressure structure is significantly less compressible than the graphitic layered phase. The substantial peak broadening that occurred as a function of pressure did not permit us to carry out detailed refinement of the diffraction data. Instead we investigated the nature of the structural changes at high pressure using density functional theory (DFT) calculations, that enabled us to gain understanding of the pressure induced transformation by comparing the predicted diffraction profiles with experiment (Fig. 3).

DFT calculations. In a first series of DFT studies we geometry-optimized the structure of $g-C_6N_9H_3 \cdot HCl$ between $P = 0$ –100 GPa in 10 GPa steps, starting each optimization from the ambient pressure lattice spacings obtained from experiment ($a, b = 8.42$ Å; $c = 6.34$ Å). We generated a proton ordered version of the 40-atom crystallographic unit cell within space group $P1$, removing all local symmetry constraints to allow the atoms to relax both within and away from the graphitic planes. This differs from our experimental data analysis that assumed a spatially averaged $P6_3/m$ unit cell^{8,18}. The proton-ordered structure exhibits a small shear distortion between adjacent planes along (010) to maximize electrostatic interactions between the H^+ and Cl^- ions within layer voids. This leads to a small separation between a and b cell parameters that increases slightly with compression but that remains insignificant until above 20 GPa (Fig. 4). At $P = 0$ GPa the optimized lattice

parameters were found to be $a, b = 8.37$ Å; $c = 6.23$ Å, slightly smaller than those found experimentally (8.42, 6.34 Å) as is typical for LDA results. During compression there is a rapid decrease in the c -axis parameter consistent with experiment: between 0–40 GPa there is a 17% reduction in c , compared with 3.7% and 5.8% in the a and b lattice parameters (Fig. 4). Between 60–70 GPa a sudden collapse of the c -axis occurred in these initial compression experiments, and then this parameter remained approximately constant up to 100 GPa (Fig. 4).

These initial results showed that a dramatic change had occurred in the structure as the c axis dimension was reduced by compression, implying a separation between the initially planar layers of approximately 2.0 Å, without considering the reduction in distances due to layer buckling. Such a small interlayer separation could lead to the onset of C-N interlayer bonding and we investigated this possibility by analyzing the fully relaxed structures as a function of densification. The results led us to identify the structure optimised at high pressure as a new phase of the material, characterized by the occurrence of bonding between a subset of sp^3 hybridized C and N atoms in adjacent layers (Fig. 5). This new phase is termed the ILB1 structure to distinguish it from the densified graphite-like phase with buckled but independent layers obtained at lower compression (ILB0). The C-N bonding occurs between atoms associated with triazine rings that in the ambient pressure phase overlapped each other in adjacent layers; the others located above and below the $C_{12}N_{12}$ voids remain sp^2 -hybridised giving rise to a unique new pillared-layered structure that contains a mixture of sp^2 - and sp^3 -bonded C and N atoms (Fig. 5).

Once we had identified the occurrence and connectivity of the new high-pressure phase, we examined the relative enthalpies of the ILB0 and ILB1 polymorphs over a wide pressure range, starting the studies using the compressed but still graphite-like (ILB0) structure obtained at 60 GPa and then gradually increasing P , compared with results during gradual decompression of the ILB1 phase obtained at 70 GPa (Fig. 6). Each calculation was initiated from the geometry-optimized structure at the immediately adjacent pressure value. The C-N connectivity was maintained throughout in both series of calculations, indicating that the ILB0 and ILB1 phases correspond to separate functions in the potential energy surface of the system and that their interconversion is an activated process that does involve interlayer

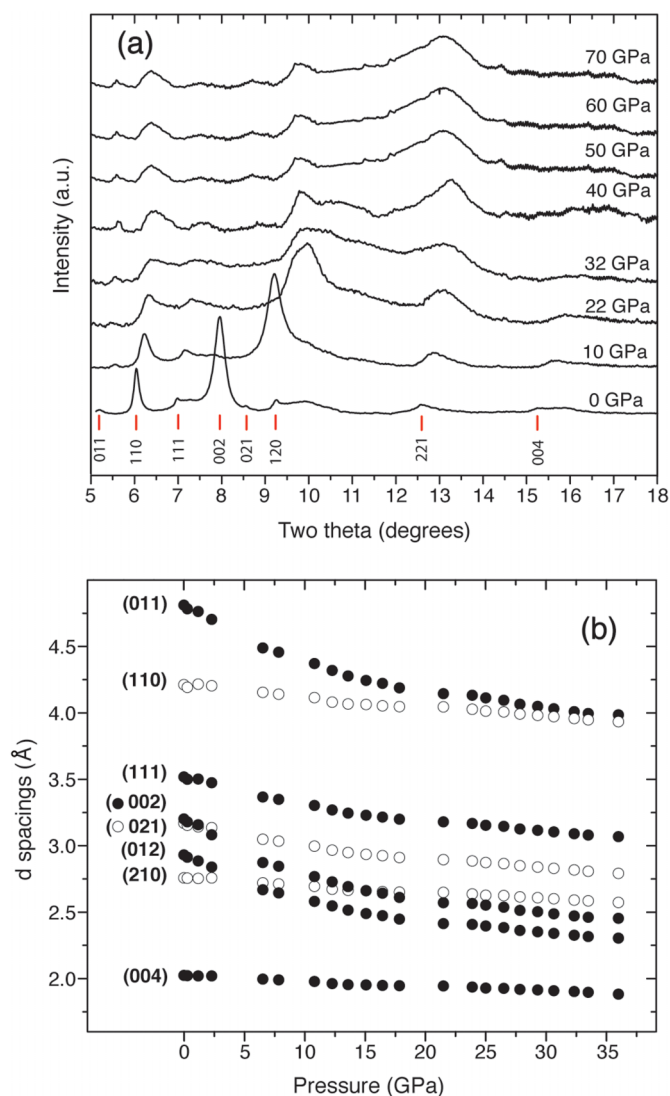


Figure 2 | Angle dispersive synchrotron X-ray diffraction data for $C_6N_9H_3 \cdot HCl$ obtained up to $P = 70$ GPa ($\lambda_o = 0.4441$ Å). Peaks of interest are labelled with hkl designations according to the $P6_3/m$ space group. (a) Selected patterns showing the onset of peak broadening for the layered phase above 10 GPa followed by the rapid emergence of the new pattern above 40 GPa. (b) Variation of d spacings measured for the principal peak maxima assigned to the low pressure graphitic phase as a function of pressure.

but not intralayer C-N bond breaking or formation. Comparing the calculated enthalpies we identified 47 GPa as the equilibrium transition pressure between the ILB0 and ILB1 polymorphs at $T = 0$ K (Fig. 6). Following the compression studies we relaxed the ILB1 structure to ambient pressure, and found that the pillared connectivity was retained. Similar calculations repeated for the hypothetical Cl-free compound showed a similar structural transformation occurring at high pressure, but with the isoenthalpic point between ILB0 and ILB1 phases reduced to ~ 5 GPa. That result indicates that varying the Cl content of these gCNM phases should cause the transition pressures and recoverability of the pillared-layered material to be adjusted experimentally.

In order to fully characterize the structural changes associated with compression of $C_6N_9H_3 \cdot HCl$ from its ambient pressure graphitic phase to the denser ILB1 polymorph at high pressure, we measured a set of dihedral angles in the minimum energy structures relaxed at each pressure. These angles (Fig. 7a) are chosen to describe

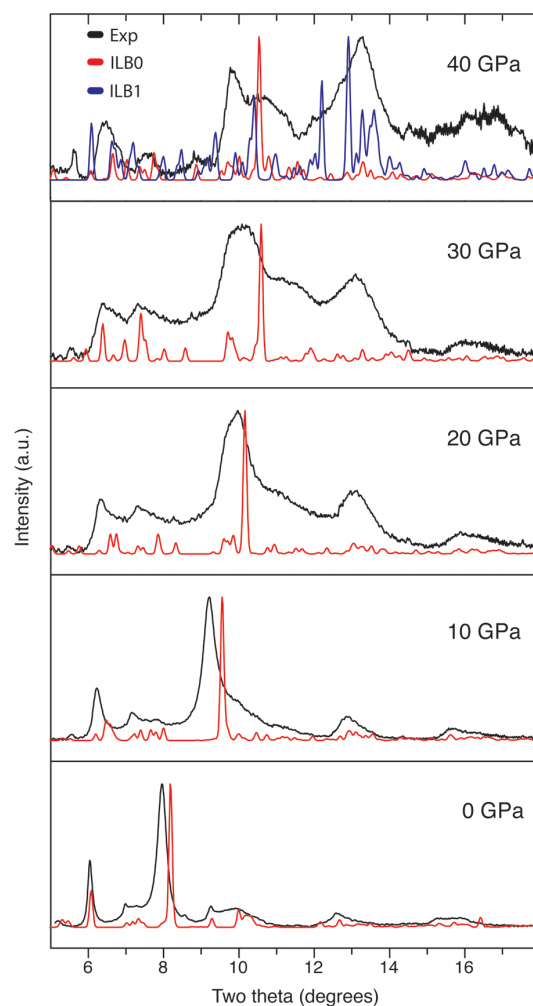


Figure 3 | Comparison of experimental (black line) with the DFT predicted (ILB0 phase, red line) X-ray patterns for the graphitic phase at various pressures. At 40 GPa the blue pattern corresponds to dense forms with interlayer bonding (ILB1) as described in the text.

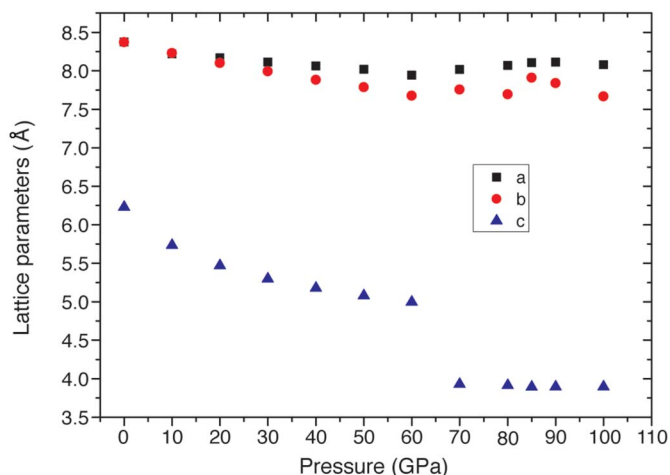


Figure 4 | Changes in the DFT calculated lattice parameters for a proton ordered version of the $g-C_6N_9H_3 \cdot HCl$ structure as a function of pressure.

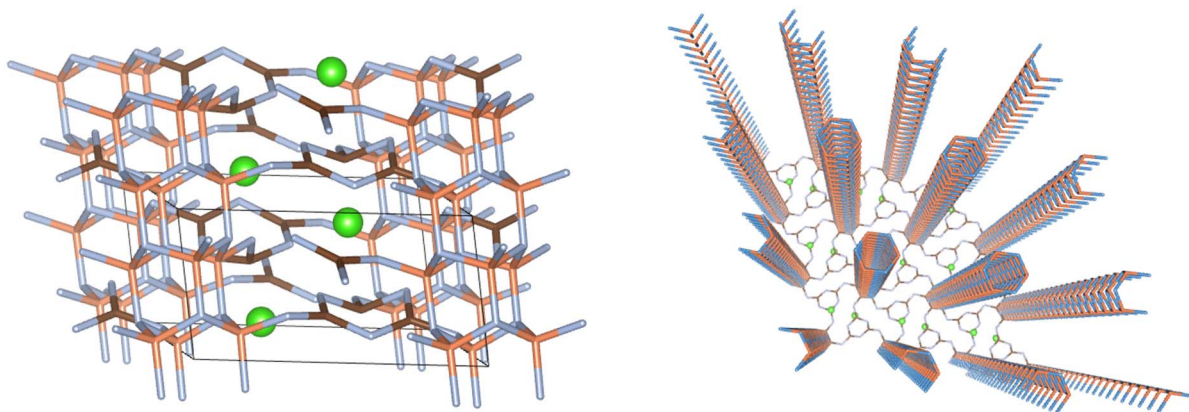


Figure 5 | Left: The ILB1 phase of $C_6N_9H_3 \cdot HCl$ obtained at high pressure from DFT calculations. In the real structure studied experimentally the Cl^- displacements above and below the layers can occur in a random or locally ordered fashion. Right: picture highlighting the formation of pillars with three-dimensional connectivity between the carbon nitride layers produced by interlayer bonding within a mixed sp^2 - sp^3 bonded state; the pillars are connected within the planes by relatively undistorted triazine rings.

the distortion of the initially planar graphitic layers: 1) the internal dihedral angle of a protonated C_3N_3 ring (ABCD); 2) the dihedral angle formed by the skeletal proton (i.e. the bridging NH group) with respect to the neighbouring triazine ring (ABFG); and 3) the internal dihedral angle of a non-protonated C_3N_3 ring (HIJK). All these values are identically zero for fully planar layers and any deviations thus record buckling of the gCNM framework. Achieving a value of 60° in any of these parameters indicates a change of hybridization at the central C and N atoms from sp^2 to sp^3 . At each pressure reported in Fig. 7 we employ the thermodynamically stable phase from the DFT calculations, i.e. ILB0 below the transition pressure of 47 GPa, and ILB1 above.

At ambient pressure the ILB0 structure is nearly planar with all dihedral angles $< 2^\circ$, as expected for a graphitic phase with delocalized sp^2 bonds. However, this condition is lost as soon as the structure is compressed even slightly. By 10 GPa the dihedral angles HIJK and ABFG differ noticeably from zero but those within the C_3N_3 rings (ABCD) remain constant. This reveals a buckling of the layers around the bridging -NH- groups (ABFG) beginning at low pressure that is accompanied by a displacement of the Cl^- ions out of the graphitic planes (Fig. 7b). Between 40–50 GPa the ABCD dihedral angle jumps from 2° to 65° , indicating the sp^2 to sp^3 hybridization

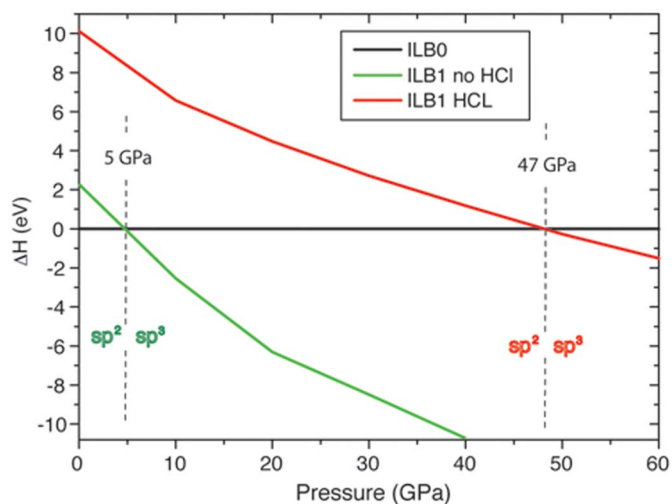


Figure 6 | Calculated enthalpy as a function of P for the layered-pillared ILB1 phase relative to the layered graphitic (ILB0) polymorph of $C_6N_9H_3 \cdot HCl$ and of the hypothetical Cl-free $C_6N_9H_3$ system.

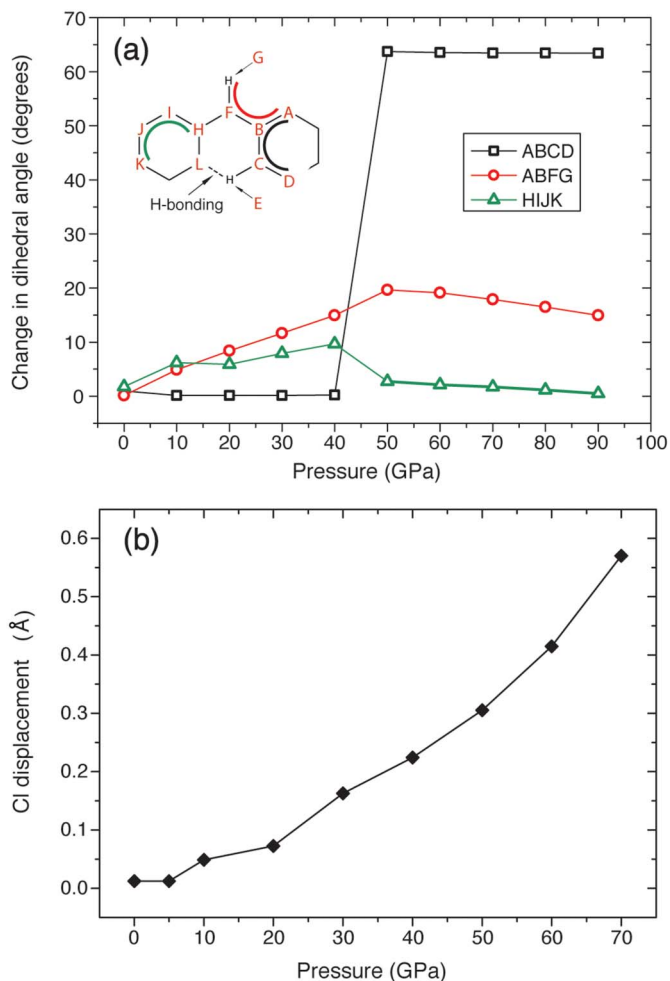


Figure 7 | (a) Dihedral angles with reference to the initially planar g- $C_6N_9H_3 \cdot HCl$ structure as a function of pressure. Here the dihedral angle changes are shown with reference to the fully relaxed and thermodynamically stable ILB0 or ILB1 states at each pressure. The structural phase transformation occurs at 47 GPa. (b) Displacement of the Cl^- ions along the c axis relative to the initial graphitic planes within the calculated ILB0 structure.



change that has taken place around the C and N atoms associated with the triazine rings. At this point the reduction in the c axis is such that the interlayer C-N bonding has occurred to yield the ILB1 structure. The structural changes can also be correlated with the behavior of the Cl^- ions. While these remain within the layers, they are clamped tightly by strong H-bonding interactions with the NH groups around the $\text{C}_{12}\text{N}_{12}$ ring sites. On application of pressure, these voids are diminished in size and they become too small to host the Cl^- ions that are progressively squeezed out of the plane. This effect becomes more marked with increasing densification until it reaches nearly 0.6 \AA by 70 GPa. These Cl^- displacements also lead to structural disorder in the real system, as the Cl^- ions can be located either above or below the planes and this effect can contribute to the peak broadening observed in the experimental X-ray diffraction patterns. Once removed from the graphitic layers and into the interlayer space the Cl^- ions also become free to be displaced along the (a, b) directions.

Comparison with experiment: ILB0 vs ILB1 formation at high pressure. Following our theoretical prediction of formation of a novel ILB1 structured phase at high pressure, we compared our calculated X-ray diffraction patterns for this material with experimental data (Fig. 8). The diffraction pattern recorded experimentally at 70 GPa showed broad features extending throughout the $5\text{--}18^\circ 2\theta$ range, that could not be refined to provide structural details. However comparison with the calculated results for the predicted ILB1 and ILB0 structures at the same pressure is revealing. The predicted X-ray pattern for the optimized ILB1 phase at 70 GPa matches the observed diffraction profile, with the main diffraction intensity concentrated near $13^\circ 2\theta$, along with other features occurring near 10° and $6.5^\circ 2\theta$. The pattern is significantly different from that expected for the ILB0 structure at the same pressure, leading us to conclude that the high pressure structural transformation observed experimentally corresponds to a transition between ILB0 and ILB1 phases.

Low pressure $V(P)$ results. The computational results enabled us not only to identify the structural features of the new high-pressure ILB1 polymorph of the carbon nitride material under study, but also to further characterize the evolution of the graphitic ILB0 phase at intermediate pressures, highlighting the occurrence of buckling distortions and displacements of the Cl^- ions. We carried out a detailed analysis of our angle dispersive X-ray diffraction data below 36 GPa to study the compression behavior of the ILB0 structure and validate the computational results in relation to the experimental measurements. Refinements were performed within $P6_3/m$ using PowderCell® software by first assigning the position of the main diffraction peak to the (002) reflection of the ABAB layer-ordered structure, using the DFT results to guide the

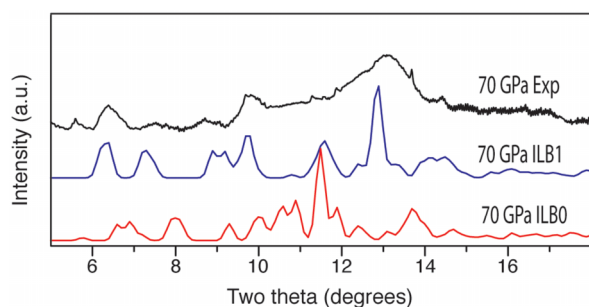


Figure 8 | Comparison of the experimental XRD pattern obtained at 70 GPa (top) vs simulated patterns generated from DFT calculations (bottom), derived from geometry optimised ILB1 and ILB0 structures of $\text{C}_6\text{N}_9\text{H}_3 \cdot \text{HCl}$, with or without interlayer bonding occurring at the same pressure.

structural analysis in the highest pressure ranges where substantial peak broadening was present (Fig. 2). The variations in refined a, b, c cell parameters led to the $V(P)$ plot shown in Figure 9.

Between 20–30 GPa we note a slight deviation of the $V(P)$ relation upwards from the expected equation of state (EoS) curve obtained by analyzing the data using the spatially averaged space group $P6_3/m$. This can occur due to layer buckling along with displacements of the Cl^- ions away from the graphitic planes, that become significant above 20 GPa as shown by the DFT results (Fig. 7b). We attempted to analyze our data in this range using lower symmetry space group solutions $P6_3$, $P6$ and $P1$ but these all gave similar R_{wp} and χ^2 values despite the increased structural degrees of freedom.

We fitted the $V(P)$ data up to 21 GPa using a third order Birch-Murnaghan (BM-3) equation of state:

$$P(V) = 3K_0 f (1 + 2f)^{5/2} \left(1 + \frac{3}{2} (K_0' - 4)f \right)$$

with K_0 the zero pressure bulk modulus and K_0' its pressure derivative, and the volume strain variable expressed by

$$f = \frac{1}{2} \left[\left(\frac{V_0}{V} \right)^{2/3} - 1 \right]$$

This fit yielded $K_0 = 32.8 \pm 7.3$ GPa and $K_0' = 4.8 \pm 0.5$, in good agreement with our DFT results for the ILB0 polymorph ($K_0 = 29.1$ GPa; $K_0' = 6.7$). The compressibility is comparable with crystalline graphite ($K_0 = 34$ GPa), although polycrystalline samples have been reported with K_0 values extending down 10 GPa¹⁹.

Fitting our DFT $V(P)$ results for the high-pressure ILB1 $\text{C}_6\text{N}_9\text{H}_3 \cdot \text{HCl}$ structure to a BM-3 EoS yields a bulk modulus $K_0 = 130 \pm 5$ GPa and $K_0' = 3.57 \pm 0.2$, clearly showing that the ILB1 structure has much lower compressibility than the sp^2 bonded graphite-like ILB0 phase ($K_0 = 29.1 \pm 4.1$ GPa). The new high pressure ILB1 phase, despite partly retaining the void intralayer structure of the low pressure ILB0 polymorph, has therefore substantially higher structural strength, a feature of potential interest for practical applications.

Discussion

We conducted a high pressure study of graphitic $\text{C}_6\text{N}_9\text{H}_3 \cdot \text{HCl}$ using complementary experimental and theoretical approaches. The

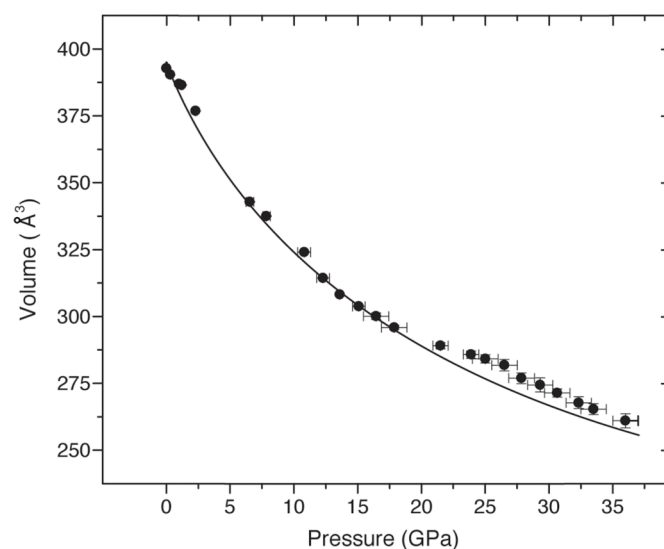


Figure 9 | $V(P)$ plot obtained from our experimental data (circles) for $g\text{-C}_6\text{N}_9\text{H}_3 \cdot \text{HCl}$ analyzed within the spatially averaged space group $P6_3/m$. The data were fitted up to 21 GPa using a third order Birch-Murnaghan equation of state ($K_0 = 32.8 \pm 7.3$ GPa and $K_0' = 4.8 \pm 0.5$) and extrapolated to 36 GPa (line).



graphitic layered compound $C_6N_9H_3 \cdot HCl$ was subjected to pressures of up to 70 GPa in a diamond anvil cell, and its structural behaviour was examined using synchrotron X-ray diffraction. The structural model proposed by Zhang et al. with a layered hexagonal ($P6_3/m$) structure was employed for the experimental data analysis, for which it provides a useful description up to a pressure of ~ 40 GPa. Close examination of the $V(P)$ relation indicates an anomaly near 20 GPa that can be explained by a deviation of the structure from $P6_3/m$ symmetry that can be interpreted from the computational results. On increasing pressure from ambient conditions, we observe three distinct structural rearrangements: at ambient pressure the carbon nitride layers are atomically flat and host the Cl^- ions within the layers; between 10–20 GPa the layers buckle and the Cl^- ions displace vertically but not horizontally with respect to the layers; above 20 GPa the Cl^- ions can displace significantly both horizontally and vertically, making the $P6_3/m$ model less and less appropriate for a detailed structural description.

The calculations identify the formation of a new pillared structure (referred to as ILB1), that is thermodynamically stable compared to the graphitic phase above 47 GPa. Simulated XRD patterns using graphitic and pillared phases from the computational work were compared with the experimental XRD data, and these indicate that the predicted pillared structure provides the most plausible match to the observed data above 40 GPa. This pillared structure is formed by buckled sp^2 -hybridized platelets joined by sp^3 -hybridised "tubes" running along the (001) direction (Fig. 5). The close match between the experimental data and that of the ILB1 structure suggests that the initially graphite-like system undergoes a change in hybridization and experiences interlayer C-N bonding as predicted by the calculations.

In conclusion, our experimental and DFT results indicate that compression of the layered compound $g-C_6N_9H_3 \cdot HCl$ at ambient temperature results in a polymorphic transformation leading to a new interlayer bonded phase. This has mixed sp^2 - sp^3 bonding between C and N atoms in adjacent layers and it gives rise to a new family of pillared-layered compounds that can combine the essential characteristics of the 2D material with buckled $C_xN_y(H_z)$ planes and the mechanical properties of a 3D-bonded compound.

Methods

The starting compound $g-C_6N_9H_3 \cdot HCl$ was formed from a 1 : 2 mixture of melamine ($C_3N_6H_6$) and cyanuric chloride ($C_3N_3Cl_3$) reacted under high-P,T conditions (1.5 GPa, 550 °C) in a piston-cylinder device. The synthesis details and structural characterization of this material were described previously^{8,18}.

Synchrotron X-ray diffraction studies were carried out at up to 70 GPa using angle dispersive techniques at ESRF ID27 (Grenoble, France; $\lambda_o = 0.3738$ Å; Figure 2). Additional data were obtained at Diamond Light Source I15, UK ($\lambda_o = 0.4441$ Å). Samples were loaded into mechanically (four post Mao-type symmetrical cells) or gas-driven He membrane diamond anvil cells (DACs). Diamonds with 200–300 μm culet sizes were used to collect data up to 70 GPa. Re gaskets pre-indented to ~ 30 μm with gasket holes ~ 80 μm in diameter were drilled by electro-erosion. Samples were packed into the cell chamber inside a glove box without a pressure-transmitting medium (PTM). Ruby fluorescence spectra indicated that the pressurisation environment remained reasonably "hydrostatic" throughout most of the runs: pressure gradients of only ~ 1 –2 GPa across the cell were detected and the ruby signals showed little broadening. The samples were loaded without a PTM to avoid interference with the weak and often broadened diffraction signals from the low-Z carbon nitride material, and to avoid potential effects associated with intercalation of fluid species such as He, N_2 or H_2 into the layered structure. X-ray diffraction data were recorded using MAR image plate or CCD detectors and analysed using Fit2D²⁰, FullProf²¹ and GSAS^{22,23} software.

Electronic structure calculations were carried out under periodic boundary conditions within the local density approximation (LDA) of density functional theory (DFT) using the planewave code CASTEP²⁴. We used ultra-soft pseudopotentials and chose the cut-off energy (450 eV) and k-point grid size ($3 \times 3 \times 4$) to obtain best converged results²⁵. Calculations were performed under hydrostatic pressure conditions: full geometry optimizations were carried out at each pressure within space group $P1$ using a 40-atom unit crystallographic cell. Prior to each geometry optimization, the atoms were subjected to small random displacements to produce symmetry-free initial structures.

1. Liu, A. Y. & Cohen, M. L. Prediction of new low compressibility solids. *Science* **245**, 841–842 (1989).

- Teter, D. M. & Hemley, R. J. Low-compressibility carbon nitrides. *Science* **271**, 53–55 (1996).
- Horvath-Bordon, E. et al. High-pressure synthesis of crystalline carbon nitride imide, $C_2N_2(NH)$. *Angew. Chem. Int. Edit.* **46**, 1476–1480 (2007).
- Salamat, A. et al. Tetrahedrally bonded dense C_2N_2H with a defective wurtzite structure: X-ray diffraction and Raman scattering results at high pressure and ambient conditions. *Phys. Rev. B* **80**, 1041066 (2009).
- Bojdys, M. J., Muller, J. O., Antonietti, M. & Thomas, A. Ionothermal Synthesis of Crystalline, Condensed, Graphitic Carbon Nitride. *Chem. Eur. J.* **14**, 8177–8182 (2008).
- Miller, D. R., Swenson, D. C. & Gillan, E. G. Synthesis and structure of 2,5,8-triazido-s-heptazine: An energetic and luminescent precursor to nitrogen-rich carbon nitrides. *J. Am. Chem. Soc.* **126**, 5372–5373 (2004).
- Wang, X. C. et al. A metal-free polymeric photocatalyst for hydrogen production from water under visible light. *Nature Mater.* **8**, 76–80 (2009).
- Zhang, Z. H. et al. High-pressure bulk synthesis of crystalline $C_6N_9H_3 \cdot HCl$: A novel C_3N_4 graphitic derivative. *J. Am. Chem. Soc.* **123**, 7788–7796 (2001).
- Ueno, M. et al. Room-temperature transition of rhombohedral-type boron nitride under high static pressure. *Phys. Rev. B* **45**, 10226–10230 (1992).
- Yagi, T. et al. High-pressure *in situ* x-ray-diffraction study of the phase transformation from graphite to hexagonal diamond at room temperature. *Phys. Rev. B* **46**, 6031–6039 (1992).
- Solozhenko, V. L. & Kurakevych, O. O. Raman scattering from turbostratic graphitelike BC_4 under pressure. *J. Appl. Phys.* **102**, 063509 (2007).
- Solozhenko, V. L. & Kurakevych, O. O. Reversible pressure-induced structure changes in turbostratic BN-C solid solutions. *Acta Crystallogr. B* **61**, 498–503 (2005).
- Mao, W. L. et al. Bonding changes in compressed superhard graphite. *Science* **302**, 425–427 (2003).
- Meng, Y. et al. The formation of sp^3 bonding in compressed BN. *Nature Materials* **3**, 111–114 (2004).
- Kroke, E. et al. Tri-s-triazine derivatives. Part I. From trichloro-tri-s-triazine to graphitic C_3N_4 structures. *New J. Chem.* **26**, 508–512 (2002).
- Kouvetakis, J., Bandari, A., Todd, M., Wilkens, B. & Cave, N. Novel synthetic routes to carbon-nitrogen thin-films. *Chem. Mat.* **6**, 811–814 (1994).
- Wirnhier, E. et al. Poly(triazine imide) with Intercalation of Lithium and Chloride Ions [$(C_3N_3)_2(NH_xLi_{1-x})_3 \cdot LiCl$]: A Crystalline 2D Carbon Nitride Network. *Chem. Eur. J.* **17**, 3213–3221 (2011).
- McMillan, P. F. et al. Graphitic carbon nitride $C_6N_9H_3 \cdot HCl$: Characterization by UV and near-IR FT Raman spectroscopy. *J. Solid State Chem.* **182**, 2670–2677 (2009).
- Krishnan, A., Dujardin, E., Ebbesen, T. W., Yianilos, P. N. & Treacy, M. M. J. Young's modulus of single-walled nanotubes. *Phys. Rev. B* **58**, 14013–14019 (1998).
- Hammersley, A. P., Svensson, S. O., Hanfland, M., Fitch, A. N. & Hausermann, D. Two-dimensional detector software: From real detector to idealised image or two-theta scan. *High Pressure Res.* **14**, 235–248 (1996).
- Rodriguez-Carvajal, J. Recent advances in magnetic-structure determination by neutron powder diffraction. *Physica B* **192**, 55–69 (1993).
- Larson, A. C. & Von Dreele, R. B. General Structure Analysis System (GSAS). *Los Alamos National Laboratory Report LAUR 86-748* (2000).
- Toby, B. H. *EXPGUI*, a graphical user interface for GSAS. *J. Appl. Cryst.* **34**, 210–213 (2001).
- Clark, S. J. et al. First principles methods using CASTEP. *Z. Kristall.* **220**, 567–570 (2005).
- Deifallah, M., McMillan, P. F. & Cora, F. Electronic and structural properties of two-dimensional carbon nitride graphenes. *J. Phys. Chem. C* **112**, 5447–5453 (2008).

Acknowledgements

Work in PFM's group has been supported by EPSRC and a Wolfson-Royal Society research merit award. The authors thank Andrea Sella, Edward Bailey, Victoria Lees, and Mohamed Matar for assistance with sample preparation, synchrotron experiments and DFT calculations. We thank Diamond Light Source (UK) and ESRF (ID27) for access to synchrotron facilities.

Author contributions

A.S. carried out experiments and analysis assisted by R.Q.C. Calculations were carried out by F.C. and M.D., P.F.M., A.S. and F.C. conceived and wrote the paper.

Additional information

Competing financial interests: The authors declare no competing financial interests.

How to cite this article: Salamat, A., Deifallah, M., Cabrera, R.Q., Corà, F. & McMillan, P.F. Identification of new pillared-layered carbon nitride materials at high pressure. *Sci. Rep.* **3**, 2122; DOI:10.1038/srep02122 (2013).



This work is licensed under a Creative Commons Attribution-NonCommercial-NoDerivs 3.0 Unported license. To view a copy of this license, visit <http://creativecommons.org/licenses/by-nc-nd/3.0>